ISSN 1674-1056
http://cpb.iphy.ac.cn
http://iopscience.iop.org/cpb
中国物理 B
Chinese Physics
中国物理 Chinese Physics B

Indium doping effect on properties of ZnO nanoparticles synthesized by sol-gel method

S Mourad, J El Ghoul, K Omri, K Khirouni

Citation: Chin. Phys. B . 2019, 28(4): 047701. **doi:** 10.1088/1674-1056/28/4/047701
Journal homepage: http://cpb.iphy.ac.cn; http://iopscience.iop.org/cpb

What follows is a list of articles you may be interested in

High uniformity and forming-free ZnO-based transparent RRAM with HfO_x inserting layer

Shi-Jian Wu(吴仕剑), Fang Wang(王芳), Zhi-Chao Zhang(张志超), Yi Li(李毅), Ye-Mei Han(韩叶梅), Zheng-Chun Yang(杨正春), Jin-Shi Zhao(赵金石), Kai-Liang Zhang(张楷亮)
Chin. Phys. B . 2018, 27(8): 087701. **doi:** 10.1088/1674-1056/27/8/087701

Effect of O-O bonds on p-type conductivity in Ag-doped ZnO twin grain boundaries

Jingjing Wu(吴静静), Xin Tang(唐鑫), Fei Long(龙飞), Biyu Tang(唐壁玉)
Chin. Phys. B . 2018, 27(5): 057701. **doi:** 10.1088/1674-1056/27/5/057701

Propagations of Rayleigh and Love waves in ZnO films/glass substrates analyzed by three-dimensional finite element method

Yan Wang(王艳), Ying-Cai Xie(谢英才), Shu-Yi Zhang(张淑仪), Xiao-Dong Lan(兰晓东)
Chin. Phys. B . 2017, 26(8): 087703. **doi:** 10.1088/1674-1056/26/8/087703

ZnO-based deep-ultraviolet light-emitting devices

Ying-Jie Lu(卢英杰), Zhi-Feng Shi(史志锋), Chong-Xin Shan(单崇新), De-Zhen Shen(申德振)
Chin. Phys. B . 2017, 26(4): 047703. **doi:** 10.1088/1674-1056/26/4/047703

Recent progress of the native defects and p-type doping of zinc oxide

Kun Tang(汤琨), Shu-Lin Gu(顾书林), Jian-Dong Ye(叶建东), Shun-Ming Zhu(朱顺明), Rong Zhang(张荣), You-Dou Zheng(郑有炓)
Chin. Phys. B . 2017, 26(4): 047702. **doi:** 10.1088/1674-1056/26/4/047702

Indium doping effect on properties of ZnO nanoparticles synthesized by sol–gel method*

S Mourad[1], J El Ghoul[1,2,†], K Omri[1], and K Khirouni[1]

[1] *Laboratory of Physics of Materials and Nanomaterials Applied at Environment (LaPhyMNE), Faculty of Sciences in Gabes, Gabes University, 6072 Gabes, Tunisia*

[2] *Imam Mohammad Ibn Saud Islamic University (IMSIU), College of Sciences, Department of Physics, Riyadh 11623, Saudi Arabia*

(Received 5 November 2018; revised manuscript received 18 February 2019; published online 19 March 2019)

Pure ZnO and indium-doped ZnO (In–ZO) nanoparticles with concentrations of In ranging from 0 to 5% are synthesized by a sol–gel processing technique. The structural and optical properties of ZnO and In–ZO nanoparticles are characterized by different techniques. The structural study confirms the presence of hexagonal wurtzite phase and indicates the incorporation of In^{3+} ions at the Zn^{2+} sites. However, the optical study shows a high absorption in the UV range and an important reflectance in the visible range. The optical band gap of In–ZnO sample varies between 3.16 eV and 3.22 eV. The photoluminescence (PL) analysis reveals that two emission peaks appear: one is located at 381 nm corresponding to the near-band-edge (NBE) and the other is observed in the green region. The aim of this work is to study the effect of indium doping on the structural, morphological, and optical properties of ZnO nanoparticles.

Keywords: In-doped ZnO nanoparticles, sol–gel process, structural and optical characterization

PACS: 77.55.hf, 78.67.Bf, 81.20.Fw, 03.75.Hh **DOI:** 10.1088/1674-1056/28/4/047701

1. Introduction

Over the last few decades, attention has been paid to the doping of semiconductor nanomaterials. Many studies on transparent conductive oxides (TCOs) have brought an important interest in nanotechnology because they may have the dual properties of having good transmittance in the visible light region and high electrical conductivity.[1] These characteristics depend on the nature, the number and the atomic arrangement of the metal cations in the crystalline oxide structure, the morphology of the nanomaterials and the presence of intrinsic (oxygen vacancies and interstitial metal) or extrinsic (doping) defects. Currently, the dominant TCOs are SnO_2, TiO_2, ZnO, and indium tin oxide (ITO). Zinc oxide is considered today to be a promising key to several nanotechnology applications. In particular, it offers good prospects as a transparent conductive oxide when doped with several types of dopants such as indium (In),[2] ytterbium (Yb),[3] molybdenum (Mo),[4] and vanadium (V).[5] The ZnO nanostructures with different morphologies have particular properties, so there is very intense interest in synthesizing the ZnO with various morphologies such as nanowires, nanorods, and nanobelts. In fact, the ZnO as a semiconductor has a wide band gap (3.3 eV), a large exciton binding energy of 60 meV at room temperature (RT),[6,7] abundance in nature and being environmentally friendly. These characteristics make this material attractive to many applications such as solar cells, optical coatings, photocatalysts, antibacterial activities, electrical devices, active medium in ultra-violet (UV) semiconductor lasers, and in gas sensors, thereby allowing faster detection and response.[8–13] The ZnO nanomaterials can be doped with transition metals (Co, Fe, Mn, Ni, *etc.*)[14–17] or with poor metals (Al, Ga, In, Sn, *etc.*),[18–21] and synthesized by several techniques (PLD, sputtering) and chemical techniques (spin-coating, pyrolysis spray, sol–gel, *etc.*). In this field, an In–ZnO material has been used in the detection of various high concentrations of VOCs,[22] solar cells,[23] and photocatalysts.[24] One has focused their attention on the application of In–ZnO in the dye-sensitized solar cells (DSSCs). The incorporation of indium into ZnONPs allows the inhibition of the recombination of photo-generated electron and holes, thus collecting more charges and enhancing the conversion efficiency values.[25]

Kim *et al.*[26] synthesized the In-doped ZnO materials via the sol–gel route. They found that when indium dopant was added to ZnO material at 0.5 mol%, it increased the carrier concentration, therefore reducing the resistivity of the materials. Zhu *et al.*[27] elaborated the In-doped ZnO nanoparticles by renovating hybrid induction and laser heating (HILH), with different mole ratios, and they found that by increasing the dopant concentration of In in ZnO, its resistance increased while its sensitivity decreases. According to that, zinc oxide has a set of physical properties that can be applied to electronics and optoelectronics. The implementation of ZnO nanoparticles manufacturing technologies has led to many applications in a wide variety fields.

Unlike glass or ceramic manufacturing processes, which

*Project supported by the Deanship of Academic Research at Imam Mohamed Ibn Saud Islamic University (IMSIU), Riyadh, Kingdom of Saudi Arabia, (Research Project Nos. 381212 and 1438H).

†Corresponding author. E-mail: Jaber.Elghoul@fsg.rnu.tn, ghoultn@yahoo.fr

© 2019 Chinese Physical Society and IOP Publishing Ltd

require very high temperatures and solid reagents, nature can create such materials in much milder conditions such as the sol–gel route. These "soft chemistry" processes make it possible to produce, from nanoparticles in solution, small objects such as films (coating), fibres, nanopowders (particles).

Therefore, in this work, we describe our approach to the synthesis of ZnO nanoparticles and study the influences of doping indium with different concentrations on the structural, morphological and optical properties of ZnO nanoparticles.

2. Experimental details

2.1. Sample preparation

ZnO and In–ZnO nanoparticles with various concentrations of indium were prepared by a sol–gel method as follows. The 16-g zinc acetate dehydrate [$ZnC_4H_6O_4.2H_2O$] (Sigma Aldrich≥99% purity) as a host precursor was dissolved in a 112-ml methanol (CH_3OH) as solvent. After 10-min magnetic stirring at room temperature, the indium chloride ($InCl_3$: Sigma Aldrich98% purity) was added as the indium dopant precursors with concentrations ranging from 0 to 5%, and continued with magnetic stirring until the total dissolution of the precursors was reached. Afterwards, the resulting solution was placed in an autoclave which had been dried by using 220-ml ethanol (C_2H_5OH) in the supercritical conditions of the latter according to the protocol of El Ghoul *et al.*[28] Even, prior to the cycle heating, we evacuated the air from inside the enclosure by using the nitrogen. The heating step was provided by temperature control of the electrically heated oven system. Inside the heart of the autoclave system there is a thermocouple-type thermometer for recording the temperature inside. When the critical temperature and pressure displayed exceeded those of the critical point of the solvent, ethanol in our case ($P = 6.3 \times 10^6$ Pa, $T = 243$ °C), we rapidly released the solvent, which is in the form of gas. Prior to cooling the system, a final nitrogen sweep was implemented necessarily in order to expel the last drops of the solvent which could remain in the autoclave so that no solvent would be condensed in the system at the moment of cooling finally. After natural cooling, Aerogel nanoparticles with good chemical homogeneity could be easily produced by this method.

2.2. Characterization techniques

The effect of indium concentration on the crystalline phase of the obtained nanoparticles was monitored with the help of Bruker D5005 powder x-ray diffractometer using Cu Kα ($\lambda = 1.5418$ Å). The recorded x-ray diffraction (XRD) patterns of ZnO and In–ZO were investigated in an angle (2θ) range from 20° to 70° in steps of 0.02°. The x-ray photoelectron spectroscopy (XPS: PHI-5702) was used to investigate the chemical and the surface binding energy states of In-doped ZnO samples. The synthesized samples were also characterized by using a transmission electron microscope (TEM) (JEM-200 CX) and an haute resolution scanning electron microscope (HRSEM) (JOEL JSM-5310 LV). The composition studies were done by energy dispersive x-ray spectrometry (EDX) that is accompanied by the TEM. The optical-absorption spectra and diffuse reflectance spectra were measured on Shimadzu (UV-3101 PC UV-Vis-NIR) spectrophotometer in a wavelength range of 200 nm–1800 nm. The powder of $BaSO_4$ was used as a standard for the optical measurements. The PL spectrophotometer (Jobin-YvonFluorolog 3-2) was used to study the intrinsic and extrinsic properties of ZnO and In–ZnO samples with an excitation wavelength of 330 nm.

3. Results and discussion

The x-ray diffraction analysis is carried out to study the crystal phases of ZnO and In–ZnO nanoparticles. Figure1shows the XRD patterns of In–ZnO nanoparticles with different indium doping concentrations. The results indicate the formation of hexagonal wurtzite phase of ZnO,[29] matched well with space group $P6_3mc$ (No. 186) (JCPDS No. 36-1451). It is clearly shown in Fig. 1 that XRD patterns of different doping concentrations are similar to XRD pattern of undoped ZnO. The values of lattice constants at room temperature of doped In–ZnO materials are agreed with those of hexagonal polycristalline wurtzite structure of ZnO ($a = 3.249$ Å and $c = 5.206$ Å.[30] This implies that the doping of In–ZnO retains the crystal structure the same as that of ZnO. In addition, when the doping rate reaches up to 4%, a secondary phase of low intensity is observed to be corresponding to In_2O_3 and which is due probably to a nucleation favored by indium with a high concentration of doping.[31] The average crystallite size D is evaluated from the Debye–Scherrer formula given as[32]

$$D = \frac{0.9\lambda}{B\cos\theta_B}, \tag{1}$$

where λ is the x-ray wavelength (1.5418 Å), θ_B is the maximum of Bragg diffraction peak and B is the full width at half maximum (FWHM) of diffracted peaks measured in radians.

As the doping concentration of In increases from 1% to 3%, the FWHM increases. However, with the doping of 4% and 5%, peaks intensity increase and become finer than those for the other samples. This is an indicator of a change in the unit cell of the hexagonal structure due to the substitution of Zn^{2+} by In^{3+}. On the other hand, shifting of these peak positions to higher angles is so clear in the dopant concentration of 5%. Indeed, we magnify the peak (002) in the inset of Fig. 1 to clearly show the shift of peak position and its FWHM. At low doping concentrations, the slight variation in the peak position with respect to the undoped ZnO peak is due to crystalline damage. While for high doping concentration, the remarkable

shift towards the high diffraction angles suggests the presence of strain in the lattice.

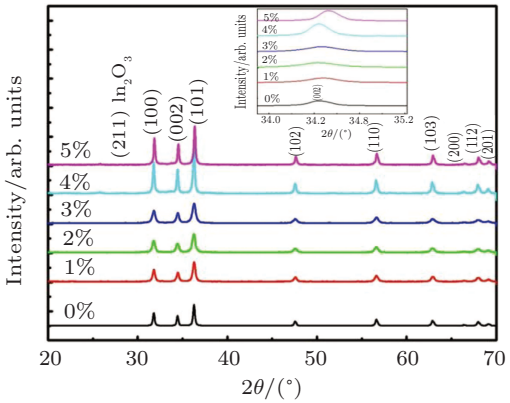


Fig. 1. X-ray diffraction patterns of indium doped and undoped ZnO, with magnified peak (002) as shown in the inset.

Table 1. Lattice parameters and crystallite sizes of the nanoparticles samples calculated from XRD.

In/at.%	*a* (101)	*c* (002)	*D*/nm
0	3.250	5.206	33
1	3.249	5.203	27
2	3.251	5.208	24
3	3.250	5.205	22
4	3.251	5.208	40
5	3.242	5.194	39

The crystallite sizes of undoped ZnO and In–ZO of different doping concentrations are calculated and summarized in Table 1. The size of undoped and In–ZO nanoparticles crystallites vary between 22 nm and 40 nm. Wang *et al.*[33] prepared the monodisperse In-doped ZnO nanomaterials by using a one-step ester elimination reaction based on alcoholysis of metal carboxylate salts, and found that the reduction in the particle size implies that the indium species play an important role in the fabricating of the nanomaterials.

The XPS analysis is used for further evaluating the purity and the chemical composition of the $In_{3\%}$–ZO and the measured spectra are shown in Fig. 2(a). The XPS survey scan reveals the presence of the binding energy of the main constituents of the ZnO crystal lattice before and after In^{3+} doping, in addition the adventitious C-1s carbon peak is detected for both samples. The asymmetric peak O-1s is observed in a region of 529 eV–533 eV (Fig. 2(b)) at about 532 eV and there is much discussion on the oxygen core level spectrum. For the case of ZnO:Al materials, an oxygen core level shows two spectral components. One component at 531.25 ± 0.20 eV is related to O^2 ions in the oxygen-deficient region in the ZnO structure,[34] and the other component at 530.15 ± 0.15 eV is estimated to be related to the O^2 ions in the wurtzite structure of the hexagonal Zn^{2+} ion array.[35] Figure 2(c) reveals the presence of two peaks centered at 1022 eV and 1045.2 eV attributed to the spin–orbit coupling of 3/2 (Zn $2p_{3/2}$) and 1/2 (Zn $2p_{1/2}$), respectively.[36,37] Figure 2(d) shows two peaks which are located at binding energy 452.34 eV and 444.85 eV corresponding to the electronic states of In $3d_{3/2}$ and In $3d_{5/2}$, respectively. The difference between these two peaks is 7.49 eV, which is corresponding well to the standard value 7.5 eV. The position of the Zn 2p and In3d peaks and their energy difference (23.2 eV and 7.49 eV) suggest that the valence state of the In and Zn ions are 3+ and 2+, respectively. These results confirm that In is successfully incorporated into the hexagonal lattice of ZnO.[38] The energy difference between the two peaks is 23.2 eV for $In_{3\%}$–ZO which is a characteristic of a Zn–O bond in a hexagonal wurtzite phase.[39]

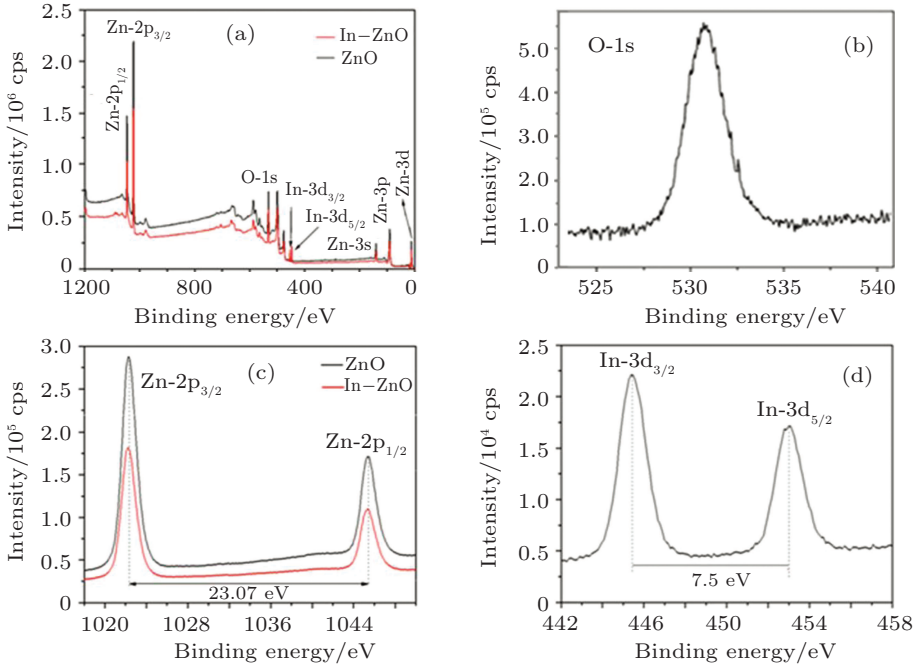


Fig. 2. XPS spectra of nanoparticles $In_{3\%}$–ZO.

The SEM observation in Fig. 3 shows that the ZnO crystallite is hexagonal in its shape and its size increases with doping concentration increasing.

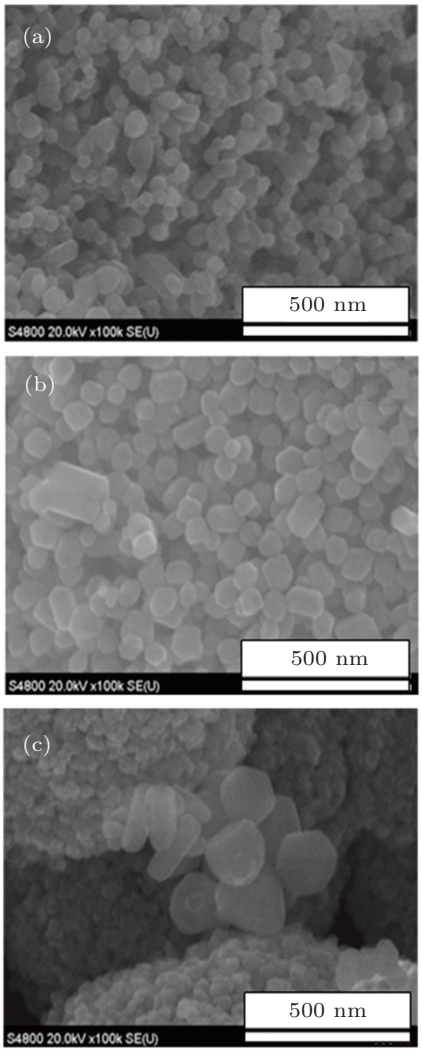


Fig. 3. HRSEM image of powders: (a) $In_{1\%}$–ZO, (b) $In_{3\%}$–ZO, and (c) $In_{5\%}$–ZO.

Figure 4 shows the TEM images of In–ZO nanopowders, the HRTEM image of ZnO and EDX analysis of doped samples. It is clearly shown that the In–ZO nanoparticles are fine and they each have a hexagonal shape at low indium concentration and shift to a cylindrical prismatic structure at high concentration with diameters ranging from 23 nm to 44 nm. The HRTEM image clearly shows that the measured distance between the planes of the fringes is 2.6 Å, which is corresponding to the plane (002) of the wurtzite structure of ZnO. Figures 4(e) and 4(f) clearly show randomly scattered diffraction spots along with ring patterns, revealing that pure (In-doped)ZnO nano-powders consist of single-(poly-)crystalline nanocrystallites. The observed diffraction spots and rings are indexed with the help of bulk ZnO JCPDS card 36-1451 data as shown in Fig. 4. The TEM analysis coupled with EDX analysis is conducted on the $In_{3\%}$–ZO sample to confirm the presence of doping element in the nanoparticles. As shown in Fig. 4, all the expected elements are detected while the presence of Cu is due to the Cu-grid used to perform this measurement.

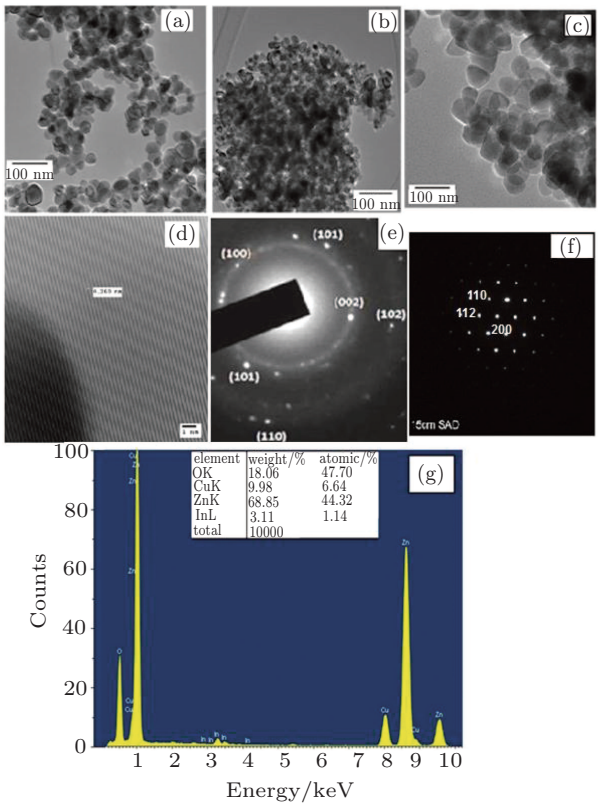


Fig. 4. TEM image of (a) ZnO, (b) $In_{3\%}$–ZO, (c) $In_{5\%}$–ZO, (d) HRTEM, and (e) SAED pattern of ZnO, (f) SAED pattern of In3%–ZO, and (g) EDX analysis.

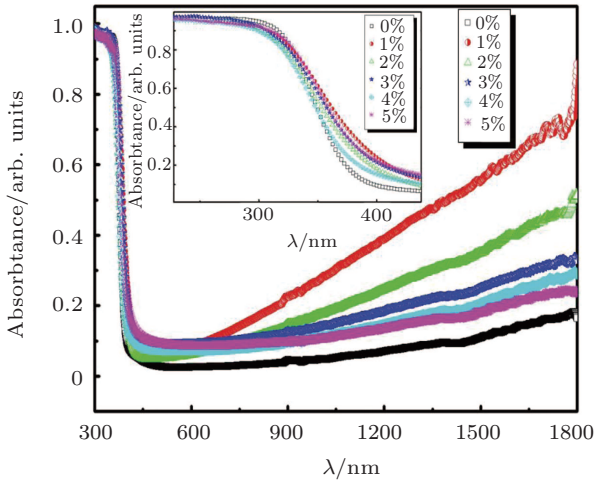


Fig. 5. UV-Vis-NIR absorption spectra of In–ZO nanoparticles for different indium doping concentrations.

In order to investigate the optical properties and band gap, the absorbance spectra of the samples are measured by using an ultra-violet-visible (UV-Vis) spectrophotometer. The absorption spectra of In–ZO nanoparticles at different concentrations of indium in UV and visible range are shown in Fig. 5. The absorption spectra of all samples prove that there

is a high absorption in the UV range (200 nm–380 nm). This result is confirmed by optical diffuse reflectance of undoped and In–ZO nanoparticles measured at room temperature and illustrated in Fig. 6. It is clear that the reflectance varies with doping concentration increasing from 3% to 4% in the UV range, which shows that the absorption is highest in this region. In contrast, the reflectance varies between 65% and 80% in the visible light region, which proves that the optical diffusion power of this type of material is quite important in this range.

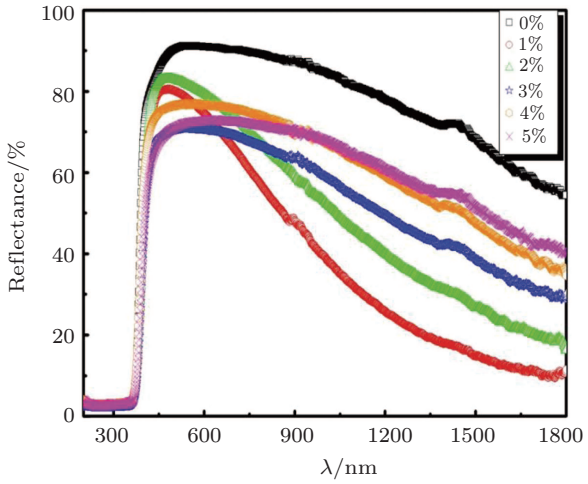


Fig. 6. UV-Vis-NIR reflectance spectra of In–ZO nanoparticles for different indium doping concentrations.

Figure 7 shows the variation of $(\alpha h\nu)^2$ for $In_{4\%}$–ZO nanoparticles with photon energy. In the case of a direct band-to-band transition, the value of $(\alpha h\nu)^2$ can be obtained from the following equation[40]

$$(\alpha h\nu)^2 = A(h\nu - E_g), \tag{2}$$

where α is the absorption coefficient, A is a constant, $h\nu$ is the photon energy, E_g is the band gap energy. A classical Tauc approach is further used to evaluate the E_g value of the as-synthesized sample. Thus, the tangent to the linear part of the curve can give a good estimate of the band gap energy for this direct transition.We notice that the gap energy of the doped ZnO sample is slightly less than that of ZnO; this can be attributed to the disorder caused by the defects in the ZnO matrix. It can be seen that the band gap energy slightly decreases with indium concentration increasing. For the doped In–ZnO sample, the spectrum shows a decrease of E_g for low indium concentration which is followed by an increase in E_g at high concentration. Kim *et al.*[41] prepared the doped ZnO materials with different In concentrations by the sol–gel process, and they found that increasing the In concentration also led to a slight improvement in the optical band gap.

In order to confirm these results, the band gap energy is estimated by using the first derivative of the reflectance $(dR/d\lambda)$.[42,43] The variation spectrum of the first derivative of the reflectance $(dR/d\lambda)$ *versus* wavelength (λ) for $In_{4\%}$–Zn nanoparticles is shown in the inset of Fig. 7. It is found that the estimated values of the band gap energy from this method are very close to those estimated by the law of Tauc (Table 2). It has been reported that the In^{3+} ions create a donor level below the conduction band which induces a curvature at the edge of the band and thus reduces the width of the band gap.[44] In addition, the decrease of gap energy can be attributed to the fact that the indium atoms are not completely absorbed by the host matrix of ZnO. So some indium atoms are positioned on the surface of the ZnO, giving rise to allowed states near the conduction band in the band gap. Similar results have been reported for Sn-doped ZnO[45] and Al-doped ZnO,[46] where the oxides SnO_2 and Al_2O_3 appear on the surfaces of the doped ZnO. For high concentrations of doping, the slight increase in gap energy may be due to the occurrence of the secondary phase In_2O_3 whose gap energy varies between 3.5 eV and 3.7 eV,[47] which is confirmed by the x-ray diffraction.

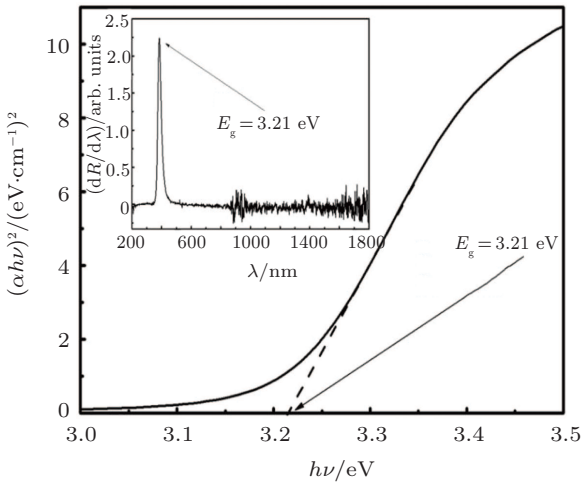


Fig. 7. Plot of $(\alpha h\nu)^2$ *versus* photon energy $(h\nu)$, with spectra of first derivative of reflectance of $In_{4\%}$–ZO nanoparticles as shown in the inset.

Table 2. Energy gaps of In–ZO nanopowders evaluated from $(\alpha h\nu)^2$ *versus* $(h\nu)$ and using first derivative of reflectance $(dR/d\lambda)$.

In/at.%	0	1	2	3	4	5
E_g/eV Tauc	3.22	3.16	3.19	3.18	3.21	3.19
E_g/eV $dR/d\lambda$	3.22	3.16	3.18	3.18	3.21	3.18

Figure 8 shows the room temperature photoluminescence spectra of the ZnO and In–ZO nanoparticles at an excitation wavelength of 330 nm. It is clear that the PL spectra exhibit an intense UV emission between 381 nm and 382 nm (3.25 eV) and a broad green–yellow emission between 544.5 nm (2.27 eV) and 565 nm (2.21 eV). The weak ultraviolet (UV) emission is assigned to the band-edge exciton of ZnO. The obtained luminescence has many fine and well-defined

lines that dominate the PL spectra, indicating that the samples have good crystallinity. On the other hand at low energy, it is found that the usual luminescence covers a wide visible range where it is generally unstructured and has a lower intensity than the band edge, and thus confirming the good crystal quality of the sample.

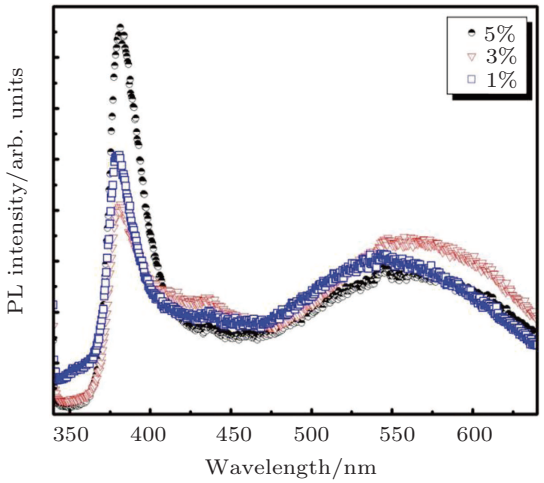


Fig. 8. PL spectra of In–ZO nanoparticles for different doping concentrations.

However, the intensity of the PL emission peak is varied by increasing the doping concentration of indium. These PL spectra show an emission UV observed at 381 nm and present the near-band edge (NBE). Kim *et al.*[29] showed that, the PL emissions of In-doped ZnO materials were dependent on In concentration where for the case of high In concentration the FWHM values of the near-band-edge emissions decrease. It is clearly shown that the fall of luminescence relative to bound excitons and relative increase of that are corresponding to free excitons (the overall decrease in luminescence intensity comes from the activation of nonradiative sites). Like the free exciton, the bound excitons can be in an excited or rotational state, giving rise to the emissions at higher energies but less likely (therefore less intense). To see the free exciton at low temperature it is necessary to have a good crystallinity of the material. However, the exciton recombinations are not only the observable radiative recombination that can be observed in a semiconductor.

From the obtained results, it can be found that a number of complex defects involved by the excessive oxygen atoms are introduced as interstitial oxygen, which is due to the charge equilibrium. Thesecomplex defects are associated with the presence of dopants in the powder and can be responsible for the green–yellow luminescence band.[40,48,49] Thereby, In3%–ZO exhibits a decrease in its UV emission peak as well as an increase in a green emission peak, indicating that it is an optimal amount of doping, allowing the separation of electrons from excited holes. This design is a focus strongly for fluent applications such as photocatalysts and this behavior has been reported by Murali *et al.*[50] The formation mechanism and the chemical nature of this defect complex will be the subject of our future study.

4. Conclusions

In this work, undopedZnO and In–ZO are synthesized by a sol–gel technique. The structural study of XRD indicates that the synthesized undoped and In–ZO nanoparticles are crystallized into a hexagonal wurtzite structure with crystallite size varying between 22 nm and 40 nm. According to TEM and HRSEM analyses, the shapes of crystallites are transformed from hexagonal to cylindrically prismatic shape with their size increasing as indium concentration increases The optical study results of ZnO and In–ZO sample reveal the presence of the intensive absorption in the UV range as well as the significant reflectance in the visible and infrared region where these results are consistent with the common behavior of ZnO nanoparticles. The band gap energy of ZnO and In–ZO are estimated from the variation of $(\alpha h\nu^2)$ with the energy of photon $h\nu$, and their values are between 3.16 eV and 3.22 eV, showing they are in good agreement with those obtained by the method of the first derivative of the reflectance. Finally, PL spectrum analyses of all samples are conducted by two intensive peaks: one is an emission UV centered at 381 nm (NBE) and the other is located in the green region. These results are of significance for using the ZnO-based photovoltaic cells as a transparent layer.

References

[1] Goto K, Kawashima T and Tanabe N 2006 *Sol. Energy Mater. Sol. Cells* **90** 3251
[2] Manoharan C, Pavithra G, DhanapandianS and Dhamodharan P 2015 *Spectrochim. Acta Part A* **49** 1
[3] Mhlongo G H, Mothudi B M, Hillie K T, Swart H C and Dhlamini M S 2015 *Mater. Lett.* **119** 71
[4] hen G, Zhao X, Zhang H, Liu F, Wang Y, Wang H, Gao J, Zhao Y, Li W and Tao J 2016 *Superlattices and Microstructures* **99** 175
[5] El Ghoul J 2015 *J. Mater. Sci: Mater. Electron.* **27** 1
[6] Yan L, Ong C K and Rao X S 2004 *J. Appl. Phys.* **96** 508
[7] E Ghoul J 2016 *Bull. Mater. Sci.* **39** 7
[8] Özgür Ü and Morkoç H 2006 *Zinc Oxide Bulk Thin Films Nanostruct.* (Elsevier) pp. 1–600
[9] Razali R, Khorsand Zak A, Majid W H A and Darroudi M 2011 *Ceram. Int.* **37** 3657
[10] Sharma P, Sreenivas K and Rao K V 2003 *J. Appl. Phys.* **93** 3963
[11] Movlarooy T and Magn J 2017 *Materials* **441** 139
[12] Dou Y, Wu F, Mao C, Fang L, Guo S and Zhou M 2015 *J. Alloys Compd.* **633** 408
[13] Hsu C L, Hsu D X, Hsueh T J, Changand S P and Chang S J 2017 *Ceram. Int.* **43** 5434
[14] El Mir L, Ben Ayadi Z, Rahmouni H, El Ghoul J, Djessas K and von Bardeleben H J 2009 *Thin Solid Films* **517** 6007
[15] El Ghoul J, Kraini M and Lemine O M 2015 *J. Mater. Sci: Mater. Electron.* **26** 2614
[16] Omri K, El Ghoul J, Lemine O M, Bououdina M, Zhang B and El Mir L 2013 *Superlattices and Microstructures* **60** 139
[17] El Ghoul J, Kraini M and El Mir L 2015 *J. Mater. Sci: Mater. Electron.* **26** 2555

[18] Hjiri M, El Mir L, Leonardi S G, Pistone A, Mavilia L and Neri G 2014 *Sens. Actuators B* **196** 413

[19] Ghiloufi I, El Ghoul J, Modwi A and El Mir L 2016 *Mater. Sci. Semicond. Process.* **42** 102

[20] Hjiri M, Dhahri R, Omri K, El Mir L, Leonardi S G, Donato N and Neri G 2014 *Mater. Sci. Semicond. Process.* **27** 319

[21] Ameen S, Akhtar M S, Seo H K, Kim Y S and Shin H S 2012 *Chem. Eng. J.* **187** 351

[22] Dhahri R, Hjiri M, El Mir L, Alamri H, Bonavita A, Iannazzo D, Leonardi S G and Neri G 2017 *Adv. Mater. Dev.* **2** 34

[23] Menner R, Cemernjak M Paetel S and Wischmann W 2017 *Thin Solids Films* **633** 239

[24] Slama R, El Ghoul J, Omri K, Houas A, El Mir L and Launay F 2016 *J. Mater. Sci: Mater Electron.* **27** 7939

[25] Chava R K and Kang M 2017 *J. Alloys Compd.* **692** 67

[26] Kim S, Kim C, Na J, Oh E, Jeong C and Lim S 2015 *J. Sol–Gel Sci. Technol.* **74** 790

[27] Zhu B L, Zeng D W, Wu J, Song W L and Xie C S 2003 *J. Mater. Sci. Mater. Electron.* **14** 521

[28] El Ghoul J, Barthou C and El Mir L 2012 *Superlattices and Microstructures* **51** 942

[29] El Ghoul J, Barthou C, Saadoun M and El Mir L 2010 *Physica B* **405** 597

[30] Omri K, Najeh I, Dhahri R, El GhoulJ and El Mir L 2014 *Microelectron. Eng.* **128** 53

[31] Prajapati C S and Sahay P P 2013 *Mater. Sci. Semicond. Process.* **16** 200

[32] Scherrer P 1918 *GöttingerNachr* **2** 98

[33] Wang Q L, Yang Y F, He H P, Chen D D, Ye Z Z and Jin Y Z 2010 *Nanoscale Res. Lett.* **5** 882

[34] Fan J C C and Goodenough J B 1997 *J. Appl. Phys.* **48** 3524

[35] Chung Y M, Moon C S, Jung M J and Han J G 2005 *Surf. Coat. Technol.* **200** 936

[36] Huang S Y, Cheng Q J, Xu S, Wei D Y, Zhou H P, Long J D, Levchenko I and Ostrikov K 2012 *J. Appl. Phys.* **111** 036101

[37] Lupan O, Emelchenko G A, Ursaki V V, Chai G, Redkin A N, Gruzintsev A N, Tiginyanu I M, Chow L, Ono L K, Roldan Cuenya B, Heinrich H and Yakimov E E 2010 *Mater. Res. Bull.* **45** 1026

[38] Mahmood K, Park S B and Sung H J 2013 *J. Mater. Chem. C* **1** 3138

[39] Bomben K D, Moulder J F, Sobol P E and Stickle W F 1995 *Handbook of X-ray Photoelectron Spectroscopy*, ed. Jill Chastain, published by Perkin-Elmer Corporation Physical Electronics Division, pp. 1–261

[40] El Ghoul J, Bouguila N, Gómez-Lopera S A and El Mir L 2013 *Superlattices and Microstructures* **64** 451

[41] Kim Y and Leem J Y 2015 *Korean J. Phys. Soc.* **66** 1516

[42] Riveros G, Gomez H, Henríquez R, Shrebler R, Cordova R, Marotti R E and Dalchiele E A 2002 *Soc. Chil. Quim.* **47** 1

[43] Henríquez R, Grez P, Muñoz E, Gómez H, Badán J A, Marotti R E and Dalchiele E A 2010 *Thin Solid Films* **518** 1774

[44] Alamdari S, Tafreshiand M J and Ghamsari M S 2017 *Mater. Lett.* **197** 94

[45] Wu C, Shen L, Yu H, Huang Q and Zhang Y C 2011 *Mater. Res. Bull.* **46** 1107

[46] Kaur G, Mitra A and Yadav K L 2015 *Prog. Nat. Sci.: Mater. Int.* **25** 12

[47] Dakhel A A 2010 *Microelectron. Reliab.* **50** 211

[48] Lin B, Fu Z and Jia Y 2001 *Appl. Phys. Lett.* **79** 943

[49] Vempati S, Mitra J and Dawson P 2012 *Nanoscale Res. Lett.* **7** 1

[50] Murali A, Sarswat P K and Sohn H Y 2019 *Mater. Today Chem.* **11** 60